九州大学大学院総合理工学府報告
第 42 巻 第 1 号 9-18 頁 令和 2 年 9 月

Engineering Sciences Reports, Kyushu University
Vol. 42, No. 1, pp. 9-18, SEP, 2020

Formation of Pt-rich AuPt Alloy Frame Nanorods with Semi-spherical End Caps Using Au Nanorods as Sacrificial Templates

Masaharu TSUJI[*1,*2†] Atsuhiko YAJIMA[*3] Yukinori NAKASHIMA[*3]
Keiko UTO[*1] Masashi HATTORI[*2] Jun-Ichiro HAYASHI[*1,*2]
Takeshi TSUJI[*4] and Hirofumi KAWAZUMI[*5]
[†]E-mail of corresponding author: tsuji@cm.kyushu-u.ac.jp

(Received July 15, 2020, accepted July 24, 2020)

Pt-rich AuPt alloy frame nanorods (NRs) with semi-spherical end caps were synthesized using Au NRs as sacrificial templates. Shape, size, and composition changes of product particles were examined by using transmission electron microscopy (TEM), TEM energy dispersed X-ray spectroscopy (EDS), and XRD patterns. Initially, Au-rich $Au_{92}Pt_8$ alloy NR cores with island-type Pt-rich $Au_{22}Pt_{78}$ alloy shell particles were prepared by reducing Pt^{4+} over Au NRs using ascorbic acid in the presence of cetyl trimethyl ammonium bromide (CTAB). After the addition of HCl and heating at 95 °C, site selective oxidative etching of AuPt alloy NRs by $Cl^- + O_2$ occurred. Then, Pt-rich $Au_{22}Pt_{78}$ alloy frame NRs with four {100} bridges and semi-spherical $Au_{90}Pt_{10}$@$Au_{22}Pt_{78}$ end caps, were formed. The formation of these AuPt alloy nanoframe structure was explained by faster etching rates of side {2,5,0}, {5,12,0}, and {110} facets of AuNRs and AuPt island particles on these high surface-energy facets than those of {100} and {111} facets with low surface energies. No AuPt frame structure was formed from decahedral island-type Au@Au_3Pt_{97} particles, because stable {111} facets of decahedral Au cores and Au_3Pt_{97} alloy shells were not etched by $Cl^- + O_2$. The results obtained from this study suggest a novel method for the formation of Pt-rich AuPt alloy frame structures and constitute new information related to their formation mechanism.

Key words: *AuPt alloy frame, Nanorod, Decahedral particles, Core-shell particles, Sacrificial template, Site selective oxidative etching*

1. Introduction

Metal nanoparticles have been used in wide areas ranging from catalysis[1)] to electronics,[2)] photonics,[3)] sensing,[4)] imaging,[5)] and medicine.[6)] The merit of these applications mainly arises from the expression of properties with strong correlations to their individual or combined physical and optical parameters, including composition (mono-, bi-, tri-, or polymetallic atoms), size, geometric shape (sphere, plates, rods and wires, or polygonal), and structure (solid, hollow, convex, concave, or porous).[7–9)]

Among many structures, metallic hollow nanostructures have received great attention because they often exhibit exceptional optical, electronic, and catalytic properties due to the increased surface area, reduced density, and broadly tunable localized surface plasmon resonance (LSPR).[10-16)]

The most popular technique for generation of such metallic hollow nanostructures with scalable hollow interior and porous walls is galvanic replacement (GR) reactions.[14-17)] GR is a redox process, in which one metal gets oxidized by ions of another metal having a higher reduction potential. The oxidized metal

*1 Institute for Materials Chemistry and Engineering
*2 Department of Applied Science for Electronics and Materials
*3 Department of Applied Science for Electronics and Materials, Graduate Student
*4 Department of Materials Science, Shimane University
*5 Department of Biological and Environmental Chemistry, Kindai University

thus acts as a sacrificial template. We have recently studied the syntheses of Ag–Au, Ag–Pd, and Ag–Pt alloy triangular nanoframes in aqueous solution using GR reactions of Ag nanoprisms with $HAuCl_4$, Na_2PdCl_4, and H_2PtCl_6.[18,19] GR reactions have also been applied to the preparation of AuAg alloy nanoframes using Ag nanorods (NRs) and nanowires as sacrificial templates.[20-22]

Oxidative etching of the interior of solid nanoparticles is an alternative method for the preparation of metallic nanoparticles with hollow structures. The most outstanding advantage of this method is that it is applicable to template metals whose standard electrode potentials (E^0) are higher than that of second metal deposited during GR. For example, GR reactions for Rh–Au and Pt–Au systems do not occur because the standard electrode potentials of Rh^{3+}/Rh, $PtCl_6^{2-}$/$PtCl_4^{2-}$, and $PtCl_4^{2-}$/Pt are lower than that of $AuCl_4^-$/Au.

		E^0 (V *vs.* SHE)	
$Rh^{3+} + 3e^-$	$\rightarrow$ Rh	0.76 eV	(1)
$PtCl_6^{2-} + 2e^-$	$\rightarrow$ $PtCl_4^{2-} + 2Cl^-$	0.68 eV	(2)
$PtCl_4^{2-} + 2e^-$	$\rightarrow$ $Pt + 4Cl^-$	0.76 eV	(3)
$AuCl_4^- + 3e^-$	$\rightarrow$ $Au + 4Cl^-$.	1.00 eV	(4)

Therefore, the formation of hollow structures of Rh and Pt by the addition of $AuCl_4^-$ ion is difficult. We have recently studied the preparation of Rh frame NRs using Au@Rh NRs as a sacrificial template in an aqueous solution.[23] We used a selective dissolution of Au NRs and Rh to form such hollow structures. The effects of each reagent on the formation of Rh frame NRs were studied. To assess the effects of the template shape, we also attempted to prepare frame structures using decahedral Au particles as a template. Based on such data, the growth mechanisms of Rh frame NRs were discussed.

In this study, the formation of Pt frame NRs is studied by using the same oxidative etching method as that used for preparation of Rh frame NRs.[23] We found that pure Pt nanoframes are not formed but Pt-rich AuPt alloy frame NRs are produced. The formation mechanism of AuPt alloy frame NRs using oxidative etching is discussed.

2. Experiment

2.1 Materials and experimental procedures

For use in this study, $H_2PtCl_6 \cdot 6H_2O$ (>98.5%), L(+)-ascorbic acid (>99.5%), cetyl trimethyl ammonium bromide (CTAB) (>99.0%), NaOH (>98%), distilled H_2O (for HPLC level), 10% HCl in water, and diethylene glycol (DEG: >99.5%) were purchased from Kishida Chemical Co. Ltd. Polyvinylpyrrolidone (PVP: Mw = 55 k in terms of monomeric units) was obtained from Aldrich Chemical Co. Inc. All reagents were used without further purification. Gold NRs in an aqueous solution involving CATB, which were prepared using a photochemical method,[24] were supplied by Dai Nippon Toryo Co., Ltd. (W4 type).

Pt shells were overgrown on Au NRs in an aqueous solution by reducing $H_2PtCl_6 \cdot 6H_2O$ by ascorbic acid in the presence of CTAB at 65 °C. In a typical synthesis, 1.33 mL of Au NRs involving 1.5 mM Au atoms in an aqueous solution, 1 mL of 10 mM $H_2PtCl_6 \cdot 6H_2O$ solution were added to 13 mL of aqueous solution involving 264 mM of CTAB. The Pt/Au molar ratio was 5 for the preparation of Au@Pt NRs. Then, 4 mL of 7.5 mM ascorbic acid was injected into the solution described above using a syringe pump at an injection rate of 33 μL/min. It took 121 min to inject all of the ascorbic acid solution. The reagent solution was kept at 65 °C for 3–12 h under continuous stirring. The final concentrations of Au atoms in Au NRs, H_2PtCl_6, CTAB, and ascorbic acid were, respectively, 0.1, 0.5, 178, and 1.55 mM.

After the formation of Au@Pt NRs, the product solution was heated at 95 °C. Then 6 mL of 5% HCl was added. The reagent solution was kept at 95 °C for 12 h to prepare Pt-rich frame structures by oxidative etching. When we examine whether Au NRs used for this study are dissolved by the addition of Cl^- ions or not, Au NRs, CTAB, and ascorbic acid with the same concentrations as those described above were dissolved in 20 mL of aqueous solution at 95 °C. Then 6 mL of 5% HCl was added. To examine whether Au NRs are dissolved or not, extinction spectra of Au NRs were observed after 1–6 h.

DEG was used as both a reductant and solvent for the decahedral Au core seed preparation.[25,26] In the process, 2 g of PVP (Mw = 55 k) was dissolved in 25 mL DEG and heated to 230 °C in the oil bath. Then 20 mg of $HAuCl_4 \cdot 4H_2O$ in 2 mL DEG was added to the above solution, which was heated at 230 °C for 10 min. The final respective concentrations of $HAuCl_4 \cdot 4H_2O$ and PVP in DEG were 1.8 and 670 mM. After centrifugal separation, Au

seeds were redispersed in 24.3 mL aqueous solution.

Decahedral Au@Pt particles were prepared using a similar method to that used for the preparation of Au@Pt NRs. 1 mL of 2 mM Au seeds and 1 mL of 20 mM $H_2PtCl_6 \cdot 6H_2O$ solution were added to 13 mL of aqueous solution involving 264 mM of CTAB at 65 °C. 7 mL of 40 mM NaOH was added to the reagent solution to keep the pH value at 7. Then 4 mL of 7.5 mM ascorbic acid was injected into the reagent solution using a syringe pump. Finally, 6 mL of 5% HCl was added and heated at 95 °C for 12 h to form frame structures.

When we examine whether decahedral Au nanoparticles are dissolved by the addition of HCl or not, decahedral Au seeds, CTAB, and ascorbic acid with the same concentrations as those described above were dissolved in 25 mL of aqueous solution at 95 °C. Then 6 mL of 5% HCl was added and heated at 95 °C for 6 h. The extinction spectra of decahedral Au particles after HCl addition was monitored at 1–6 h.

2.2 Characterization of nanoparticles

Shape, size, and composition of product particles were examined by using transmission electron microscopy (TEM) and TEM energy dispersed X-ray spectroscopy (EDS) (200 kV, JEM-2100F; JEOL). Samples for TEM and TEM-EDS observations were obtained by centrifuging the colloidal solution three times at 15,000 rpm for 30 min. XRD patterns of the samples were measured using Cu Kα radiation operating at 50 kV and 300 mA (RINT-TTR III, Rigaku Corp.). Extinction spectra of the product solutions were measured in the 300–1200 nm region using a spectrometer (UV-3600; Shimadzu Corp.).

3. Results and discussion

3.1 Formation of Pt frame NRs from Au@Pt NRs

3.1.1 Oxidative etching of Au NRs by the addition of HCl

It is known that Au metals are etched in an aqueous solution by the addition of Cl^-.[14-16,23] To ascertain whether Au NRs used in this study are truly dissolved by the addition of Cl^- ions or not, we monitored changes in SPR band of Au NRs after the addition HCl to the Au NR solution (Fig. 1a). The SPR band of Au NRs is observed in the 300–1200 nm region, with a longitudinal SPR band at about 900 nm with full width at half maximum (FWHM) of about 200 nm and a weak transverse SPR band at about 510 nm.[27,28] With increasing etching time from 0 h to 4 h, the main peak shifts slightly from 900 nm to 880 nm because of slight shortening of Au NRs and its intensity decreases to about half. After 6 h, the peak almost disappeared, and a weak broad band was observed in the 650–1200 nm region. These results indicate that Au NRs are etched oxidatively by the addition of HCl in our conditions.

3.1.2 Formation of AuNR@AuPt particles

Figures 2a–2e portray TEM images of Au NRs and the change in morphology that occurred when Pt^{4+} was reduced over Au NRs for 3–12 h. The average length and diameter of Au NRs are 50 nm and 5 nm, respectively, so

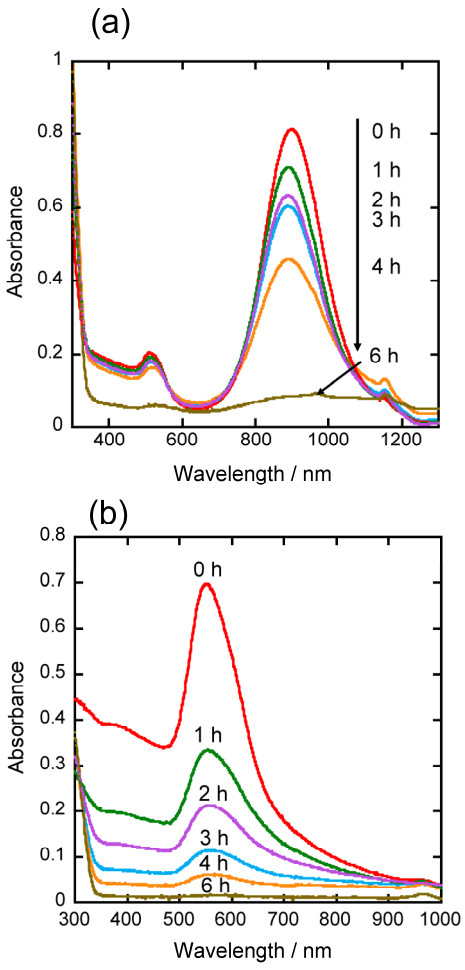

Fig. 1. Time evolution of plasmom resonance band of (a) Au NRs and (b) decahedral Au nanoparticles in an aqueous solution in the presence of CTAB after the addition of HCl.

that the aspect ratio is about 5. At a short reaction time of 3 h, small spherical island-type particles with an average diameter of about 3 nm are grown over two top and bottom edges of Au NRs. At 6 h, the average size of island particles on the top and bottom edges increases to about 5 nm, and additional island particles are formed on side facets of Au NRs. At 9–12 h, more island particles are grown over all top and bottom and side facets of Au NRs.

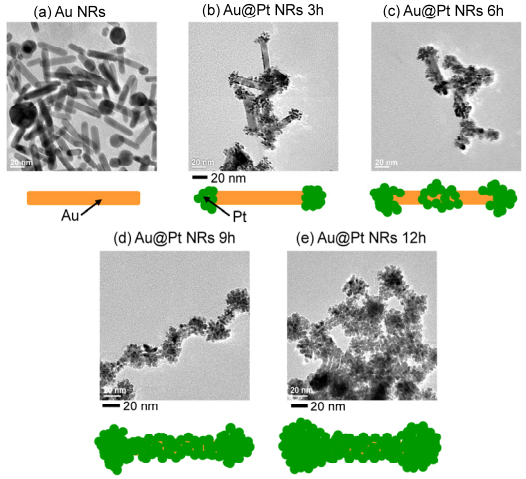

Fig. 2. TEM images of (a) Au NRs and (b)–(e) Au@Pt NRs at reaction times of 3–12 h.

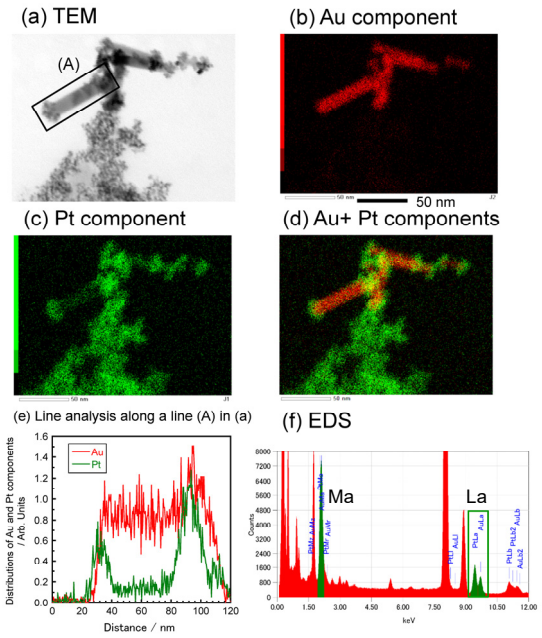

Fig. 3. TEM and TEM-EDS images of Au@Pt NRs obtained at 6 h and line analysis along a broad line (A) in Fig. 3a.

To examine what metals contribute to these morphology changes, TEM–EDS images and line analyses along each line are made for particles obtained after HCl addition for 6 h and 12 h (Figs. 3 and 4). Symbols AuMa, PtMa, AuLa, and PtLa shown in Fig. 3f according to the notation of JEOL are usually denoted by AuMα, PtMα, AuLα, and PtLα, respectively. In the EDS analysis of Au–Pt bimetallic system, it was difficult to separate Au and Pt components using the most intense AuMa and PtMa peaks at 1.9–2.3 eV (Fig. 3f). Although intensities of the second AuLa and PtLa peaks at 9.3–9.9 eV are weaker than those of the first AuMa and PtMa ones, they are well separated. Therefore, we used weaker AuLa and PtLa EDS peaks to show Au and Pt components of Au–Pt bimetallic particles in this work.

Figures 3a-3e show that Au NRs are dominantly covered by island-type Pt shells over the two top and bottom edges after 6 h, and only a small amount of Pt component is deposited on side edges of Au NRs. Figs. 4a-4e indicate that Au NRs are fully covered by island-type Pt particles with shell thickness of about 20 nm after 12 h. It should be noted that a weak Au component exists outside the Au NRs (see two blue circles in Fig. 4e). The Au component extends from Au NR core to the outer edge of Pt shell component. These EDS data imply that island-type spherical particles are not composed of solely Pt component, but a small amount of Au component (~10%) is

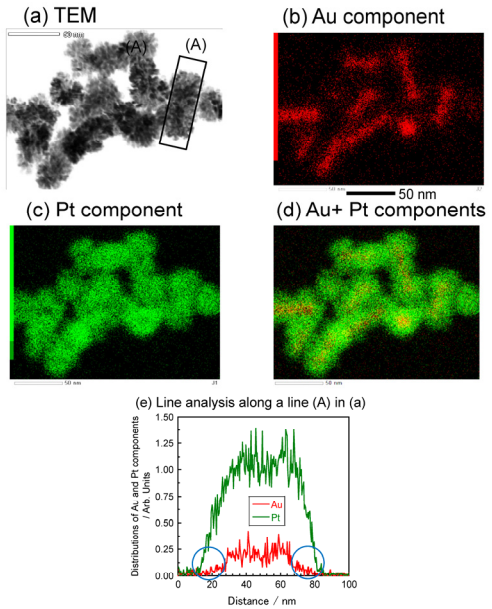

Fig. 4. TEM and TEM-EDS images of Au@AuPt NRs obtained at 12 h and line analysis along a broad line (A) in Fig. 4a.

involved in the Pt shell particles. It is reasonable to assume that during Pt island-shell formation, etching of Au NRs by $Br^- + O_2$ pair[15,23] and reduction of Au(I)/(AuIII) to Au^0 occur simultaneously. Therefore, Pt-rich AuPt alloy shells are formed over Au NRs. On the base of above TEM-EDS data, reduction of Pt^{4+} over Au NRs by using ascorbic acid in the presence of CTAB does not give AuNR@Pt particles but AuNR core Pt-rich AuPt alloy shell (AuNR@AuPt) particles.

3.1.3 Formation of AuPt frame NRs from AuNR@AuPt particles

To form Pt or AuPt frame NRs from AuNR@AuPt particles, we attempted selective etching of Au component in AuNR@AuPt particles by the addition of HCl. Fig. 5a shows a typical TEM image of Au–Pt products after 12 h etching, where frame structures with semi-spherical end caps are observed. Fig. 5b displays expanded TEM images of AuPt frame NRs, which are composed of two or three bridge edges, depending on the view angle. It is concluded that the AuPt frame NRs really consist of four bridges as shown in right figures in Fig. 5b. A similar four bridge structure was observed for Rh frame NRs formed from AuNR@Rh.[23]

Figures 6a–6f depict TEM and TEM–EDS images of Au–Pt products after 12 h etching and their line analysis data. The formation of Au–Pt frames from AuNR@AuPt particles was confirmed from these EDS data. Frame structures consist of AuPt alloy frame NRs with semi-spherical Au core Pt-rich AuPt shell end caps. No evidence of the formation of pure Pt frame NRs was observed from these EDS data. It should be noted that Pt-rich AuPt frame brides do not consist of a series of AuPt island particles, but they are composed of smooth AuPt NRs (see also Fig. 5). The average diameter of each AuPt bridge was about 5 nm. This indicates that during oxidative etching, island-type small spherical AuPt alloy particles over side facets of AuNRs coalesce with each other, leading to rod-type particles with smooth surfaces. After oxidative etching, Pt-rich AuPt shell end caps consist of larger island-type particles than those of island-type shell particles in original AuNR@AuPt particles. This suggests that coalescence of small island-type Pt-rich AuPt

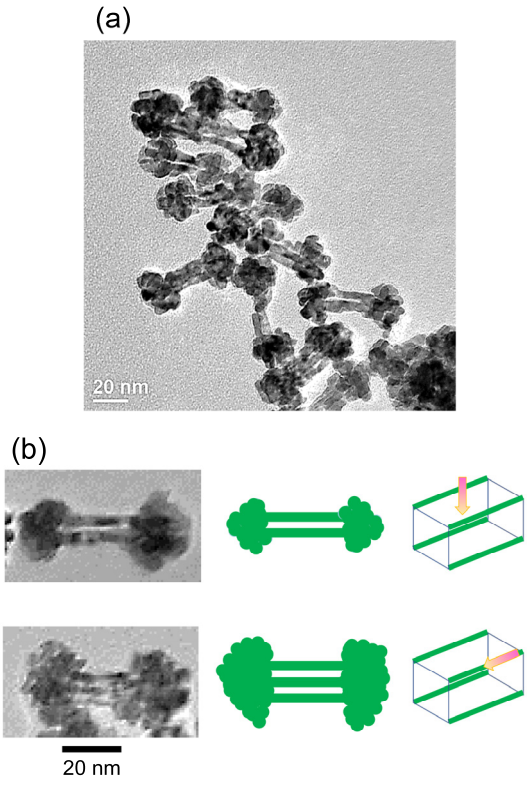

Fig. 5. (a) TEM image of Pt rich-AuPt alloy frame NRs obtained after HCl addition for 12 h. (b) Expanded TEM images of AuPt frame NRs with two or three bride edges and their frame structures observed from two different view angles.

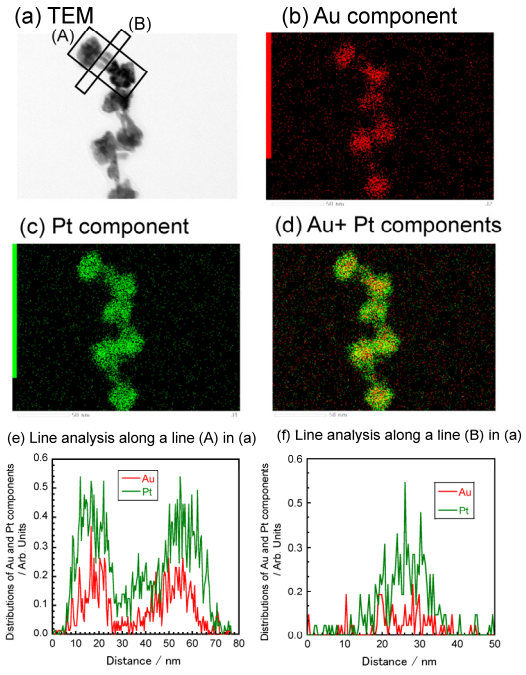

Fig. 6. TEM and TEM-EDS images of Pt-rich AuPt alloy frame NRs obtained after HCl addition for 12 h and line analysis along broad lines (A) and (B) in Fig. 6a.

particles also occurs for end cap shells, so that larger island-type particles are formed on the end caps.

The following oxidative etching processes participate in the formation of AuPt nanoframes from AuNR@AuPt.[14-16,23)]

$$\text{Au} + 1/2O_2 \xrightarrow{+\,Cl^-} \text{Au(I)/Au(III)} + O^{2-} \quad (5)$$

$$\text{Au} + 1/2O_2 \xrightarrow{+\,Br^-} \text{Au(I)/Au(III)} + O^{2-} \quad (6)$$

$$\text{Pt} + 1/2O_2 \xrightarrow{+\,Cl^-} \text{Pt(II)/Pt(IV)} + O^{2-} \quad (7)$$

$$\text{Pt} + 1/2O_2 \xrightarrow{+\,Br^-} \text{Pt(II)/Pt(IV)} + O^{2-} \quad (8)$$

AuPt alloy particles on specific Au NR surfaces remained after oxidative etching, leading to four bridge edges with semi-spherical end caps. Not only dissolution of Au NR cores and Pt-rich AuPt alloy island-type shells by above oxidative etching, but also coalescence of small island-type Pt-rich AuPt particles and atomic rearrangement within them occur, resulting in smooth AuPt alloy bridge surfaces.

3.1.4 XRD analyses of AuNR, AuNR@AuPt and AuPt nanoframes

To obtain information on crystal structures of Au NRs, AuNR@AuPt, and AuPt alloy nanoframes in more detail, powder XRD patterns were measured. Fig. 7 shows their XRD patterns in the 2θ = 30–90° range, and Fig. 8a displays expanded XRD patterns in the 2θ = 60–75° range as a typical example. The XRD patterns of Au NRs consist of single component, indicating that the presence of the crystalline gold with fcc structure (2θ equals 38.19°, 44.39°, 64.59°, and 77.59°) corresponding to {111}, {200}, {220}, and {311} planes, respectively. As demonstrated in Fig. 8a, XRD pattern of AuNR@AuPt consists of two components. They are a major peak and a weak shoulder peak at smaller angles. The major peaks were observed at 39.26°, 45.78°, 66.76°, and 80.64° in Fig. 7. These peaks shift to smaller angles by 0.48°, 0.43°, 0.66°, and 0.57° from standard peaks of crystalline platinum with fcc (39.74°, 46.21°, 67.42°, and 81.21° for {111}, {200}, {220}, and {311} planes, respectively). Thus, the major peaks can be attributed to Pt-rich AuPt alloy peaks, which is consistent with the TEM-EDS observation. Weak shoulder peaks are observed at slightly higher angles than those of pure gold peaks due to intermixing of small amount of Pt component with the major Au component. Assuming complete mixing between Au and Pt atoms in AuPt alloys, atomic ratios of Au and

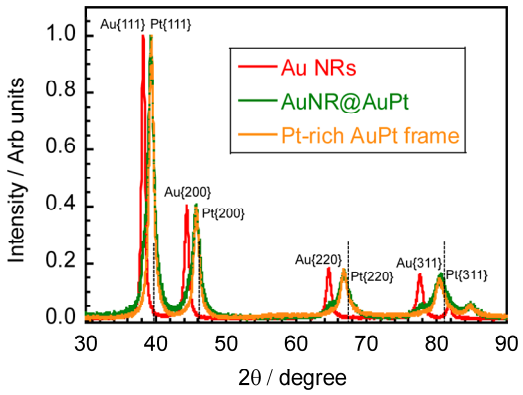

Fig. 7. XRD patterns of Au NRs, AuNR@AuPt, and Pt-rich AuPt nanoframes before analysis using Vegard's raw. Dotted lines show standard positions of fcc Pt metals.

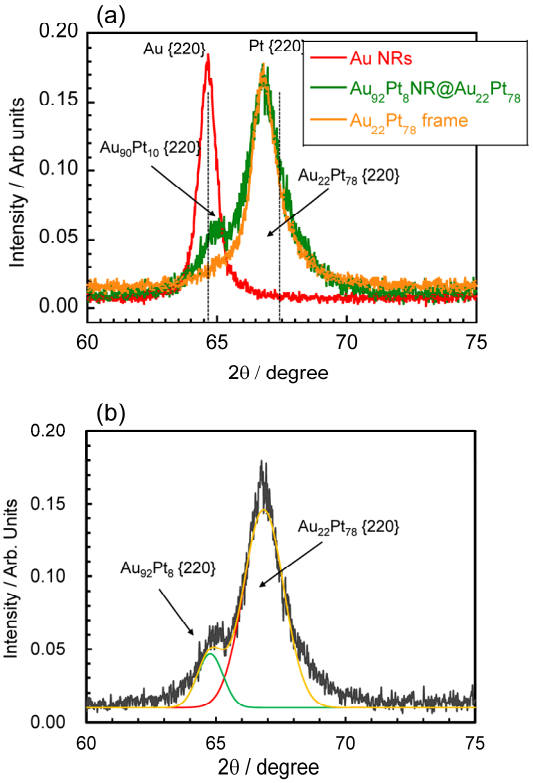

Fig. 8. (a) Expanded XRD patterns of Au NRs, AuPtNR@AuPt, and AuPt nanoframes after analysis using Vegard rule. Dotted lines show standard positions of fcc Au and Pt metals. (b) deconvolution of XRD peak of AuPtNR@AuPt using two Gaussians curves.

Pt in AuPt alloys were estimated from {220} peaks using Vegard's law (Fig. 8a).[29] By deconvoluting XRD peaks (Fig. 8b), peak positions of Au-rich AuPt alloy and Pt-rich AuPt alloy were estimated to be, respectively, 66.9° and 64.7°. From these values, the compositions of Au-rich AuPt alloy and Pt-rich AuPt alloy were evaluated to be $Au_{90}Pt_{10}$ and $Au_{22}Pt_{78}$ alloys, respectively. On the basis of above facts, it is concluded that Au NR cores consist of Au-rich $Au_{90}Pt_{10}$ alloys, whereas Pt island-shells are composed of Pt-rich $Au_{22}Pt_{78}$ alloys.

After oxidative etching, Au-rich AuPt alloy peak at about 64.7 eV becomes weak. However, deconvolution of XRD peaks of {220} facets of AuPt alloy frames gave the same peak positions for both weak Au-rich AuPt alloy shoulder peak and strong main Pt-rich AuPt alloy peak (not shown in Fig. 8b). These results suggest that the composition of major Pt-rich $Au_{22}Pt_{78}$ alloy component, which constitutes side bridge frame structure, are unchanged before and after oxidative etching. At the same time the composition of minor Au-rich $Au_{90}Pt_{10}$ alloy composition, which constitutes residual cores of semi-spherical end caps, is also unchanged before and after oxidative etching.

We have prepared AuPt alloy frame NRs using Au NRs as a sacrificial template. Fig. 9a shows the most probable crystal structure of Au NRs, which consist of eight equivalent high-index {2 5 0} or {5 12 0} facets and additional eight facets of alternative {110} and {100} facets located between two {2 5 0} or {5 12 0} facets.[23,30-33] The NR ends are terminated by the {100} facet, and side facets and end facets are combined with eight facets of alternative {110} and {111} facets. The most outstanding feature of Au NRs is that they have not only low-index facets but also high-index facets.

The surface facets play an important role in determining the shape of a nanocrystal. The formation of surface facets is essentially driven by total interfacial free energy. Owing to different density of atomic steps, ledges, and kinks, fcc facets have different surface energies. In general, the surface energy of the three typical low-index facets of an fcc metal follows the trend of $\gamma\{111\} < \gamma\{100\} < \gamma\{110\}$.[14,15] The surface energies of high-index {2 5 0} and {5 12 0} facets are expected to be much higher than those of above three low-index facets.

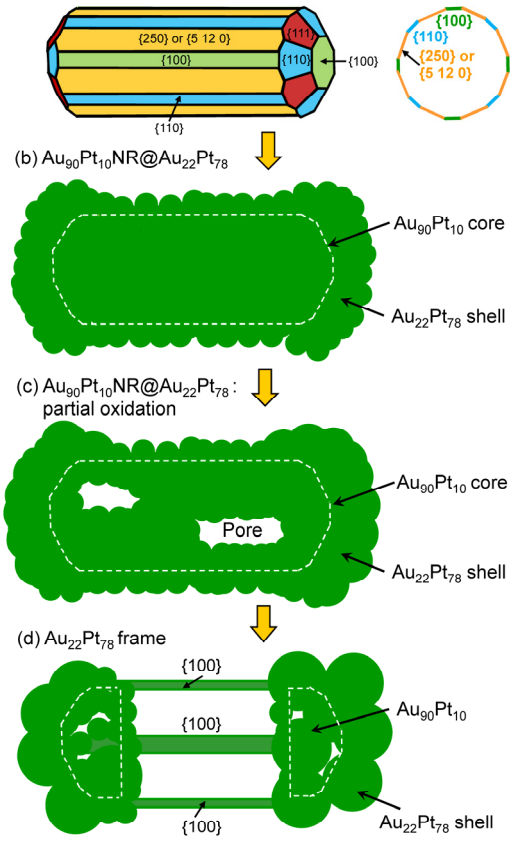

Fig. 9. Crystal structure of Au NR and formation mechanism of Pt-rich $Au_{22}Pt_{78}$ frame NR from $Au_{90}Pt_{10}$NR@$Au_{22}Pt_{78}$ by oxidative etching.

Figures 9b–9d show the formation mechanism of Pt-rich $Au_{22}Pt_{78}$ alloy frame NR with Au-rich $Au_{90}Pt_{10}$@$Au_{22}Pt_{78}$ alloy end caps. A relatively large lattice mismatch (3.8%) exists between fcc Au (lattice constant = 0.4078 nm) and Pt (0.3924 nm). In addition, Au NRs have unstable high-index facets such as {2 5 0} or {5 12 0}. Therefore, layered growth of Pt shell over Au NR is difficult, so that island-type small spherical Pt particles without distinct facets are grown over Au NRs (Fig. 9b). During island growth of Pt particles, oxidative etching of Au NRs by $Br^- + O_2$ and reduction of Au^+ and/or Au^{3+} and Pt^{4+} ions to Au^0 and Pt^0 by ascorbic acid occur simultaneously. Therefore, intermixing between Au and Pt atoms takes place, leading to Au-rich $Au_{90}Pt_{10}$NR alloy core and Pt-rich $Au_{22}Pt_{78}$ alloy shell particles ($Au_{90}Pt_{10}$NR@$Au_{22}Pt_{78}$).

By the addition of HCl, Cl^- ions and O_2 dissolved in the reagent solution penetrate into the interspace, and both $Au_{90}Pt_{10}$ NR cores and Au_{22}@Pt_{78} island shells are etched

through reactions (5) and (7). Then, a few pores are formed (Fig. 9c), and finally four bridge frame structure with semi-spherical end caps are produced (Fig. 9d). During oxidative etching, surfaces of bridges become smooth and small island-type Pt-rich $Au_{22}Pt_{78}$ particles in the end caps become large by mutual coalescence.

Since the surface energy of metals depends on not only facets but also metals, oxidative etching is expected to exhibit specific selectivity toward different facets and metals. It is expected that etching rates of high-energy {2 5 0}, {5 12 0}, and {110} facets of Au are faster than those of low-energy {100} and {111} facets of Au. Therefore, facet selective oxidative etching occurs, leaving low-energy {100} and {111} facets. On the other hand, the final formation of Pt-rich $Au_{22}Pt_{78}$ frame structures by the faster oxidative etching of Au-rich $Au_{90}Pt_{10}$ alloy cores suggests that oxidative etching rate of Au component is faster than that of Pt component under the present experimental conditions, even though Au-rich cores are covered by Pt-rich shells. This means that passivation of Pt-rich $Au_{22}Pt_{78}$ alloy shells is not so important for the oxidative etching of Au-rich $Au_{90}Pt_{10}$ alloy cores, because Cl^- and O_2 etchant pairs can easily penetrate into the interfaces of Pt-rich AuPt alloy shells.

Although etching rate of Pt component is slower than that of Au one, most of Pt-rich Au_{22}@Pt_{78} island-shell particles are also etched by $Cl^- + O_2$. However, the etching rate depends strongly on the underlying facets of Au-rich $Au_{90}Pt_{10}$ NR cores. The etching rates of Pt-rich $Au_{22}Pt_{78}$ island-shell particles over side {100} facets of $Au_{90}Pt_{10}$ NRs are slower than those over {2 5 0}, {5 12 0}, and {110} facets. Therefore, four $Au_{22}Pt_{78}$ frame bridges are left (Fig. 9d). During oxidative etching, mutual coalescence and atomic rearrangement of Pt-rich $Au_{22}Pt_{78}$ island-shell particles occurs to reduce total surface energies of products. As a result, boundaries of island particles disappear and rather smooth frame bridges are formed.

Stable {100} and {111} facets are major facets of the top and bottom edges of $Au_{90}Pt_{10}$@$Au_{22}Pt_{78}$ NRs. Therefore, etching rates of Pt-rich $Au_{22}Pt_{78}$ island particles over these stable facets are slow, so that they remain as semi-spherical $Au_{90}Pt_{10}$@$Au_{22}Pt_{78}$ particles (Fig. 9d). During oxidative etching, coalescence of small island-type Pt-rich AuPt particles occurs, so that larger island particles are grown.

3.2 Attempt for the formation of Pt frames from decahedral Au@Pt nanoparticles

3.2.1 Decahedral Au@AuPt nanoparticles produced from Au decahedra as seeds

To examine the formation mechanism of Pt-rich AuPt alloy nanoframes, we examined the effects of morphologies of Au cores for the formation of Pt-rich AuPt alloy nanoframes using decahedral Au seeds. Pt^{4+} ions were reduced in the presence of decahedral Au cores under the same experimental conditions as those used for Pt-rich $Au_{22}Pt_{78}$ frames from $Au_{90}Pt_{10}$@$Au_{22}Pt_{78}$ NRs. Figs. 10a and 10b show typical TEM images of Au decahedral particles and Au@Pt particles before HCl addition, respectively. Although Pt shells do not form layered structures, Au decahedral particles are covered by small spherical island-shell particles, as in the case of $Au_{90}Pt_{10}$@$Au_{22}Pt_{78}$ NRs.

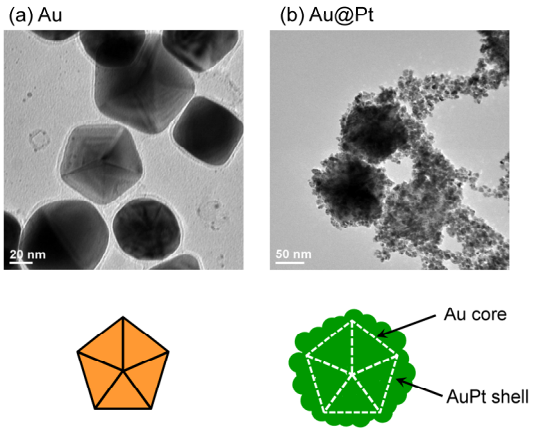

Fig. 10. TEM images of decahedral (a) Au and (b) Au@Pt particles.

Figures 11a-11e show TEM, TEM-EDS, and line analysis data of decahedral AuNR@Pt particles. Results show that a small amount of Au component (~3%) is involved in Pt island-type spherical shell particles. Therefore, small island-type spherical shell particles are not composed of pure Pt particles but they consist of Pt-rich Au_3Pt_{97} alloy particles. A low Au content in AuPt alloy arises from slower etching rate of decahedral Au particles than that of Au NRs with unstable facets.

3.2.2 Attempt for the formation of Pt nanoframes from decahedral Au@AuPt nanoparticles

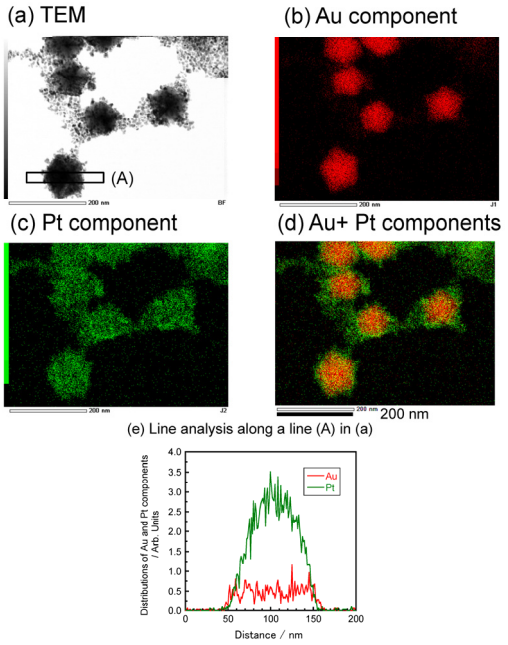

Fig. 11. TEM and TEM-EDS images of Au@AuPt and line analysis along a broad line (A) in Fig. 11a.

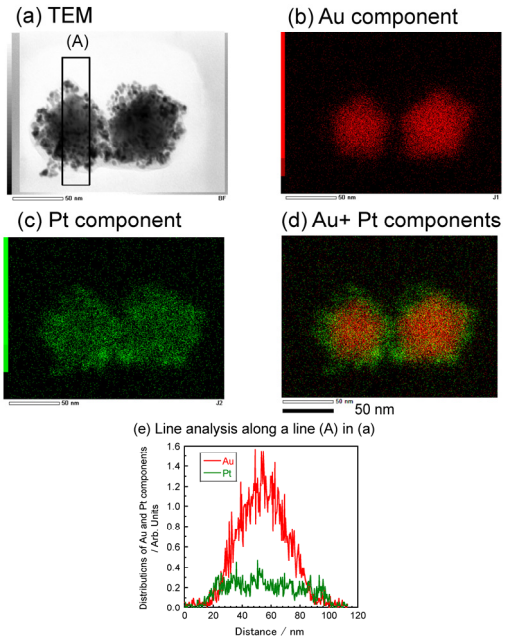

Fig. 12. TEM and TEM-EDS images of Au@AuPt obtained after HCl addition for 12 h and line analysis along a broad line (A) in Fig. 12a.

Upon examining oxidative etching of Au decahedral particles by the addition of HCl, it was found that they are dissolved as in the case of Au NRs (Fig. 1b). This indicates that decahedral Au nanoparticles can be etched as in the case of Au NRs by the addition of HCl.

We have examined whether frame structures are formed after addition of the same amount of HCl as that used for the preparation $Au_{22}Pt_{78}$ frame NRs from $Au_{90}Pt_{10}$@$Au_{22}Pt_{78}$ NRs. It is noteworthy that no frame structure can be formed as presented in Fig. 12a. Figs. 12b-12e show TEM-EDS images and its line analysis data. Results show that little shape and size changes occur for decahedral Au@Au_3Pt_{97} particles with an average diameter of ~80 nm after HCl addition. The most probable reason for non-occurrence of oxidative etching for decahedral Au@Au_3Pt_{97} particles is that Au_3Pt_{97} shells over low index Au {111} facets are too stable to be etched. Therefore, no frame structure is formed from decahedral Au@Au_3Pt_{97} nanoparticles. This is consistent with the remaining semi-spherical $Au_{90}Pt_{10}$@$Au_{22}Pt_{78}$ end caps over top and bottom edges with {111} facets. Based on the effects of facts presented above, surface energies of metallic facets play important roles in frame structure formation via facet selective oxidative etching.

4. Summary and Conclusion

Formation of Pt-rich AuPt alloy frame NRs with semi-spherical end caps was examined using Au NRs as sacrificial templates. AuPt alloy frame NRs were prepared through a two-step process in which $Au_{90}Pt_{10}$@$Au_{78}Pt_{22}$ alloy particles were initially prepared using ascorbic acid in the presence of CTAB. Then they were etched by the addition of HCl. As a result, $Au_{22}Pt_{78}$ NR frame structures with semi-spherical $Au_{90}Pt_{10}$@$Au_{22}Pt_{78}$ end caps were formed. The formation of $Au_{22}Pt_{78}$ NR frames over Au {100} facets was explained by their lower surface energies than those of other facets with fast etching rates.

To obtain information related to effects of shape of Au core for the formation of Pt-rich AuPt frame NRs, decahedral Au@Au_3Pt_{97} particles were prepared. No frame structure was formed after the HCl addition. It was explained by the slow etching rate of low-index {111} facets with the lowest surface energy. Results obtained in this study suggest a new synthesis method of unique Pt-rich AuPt alloy frame structures at a low reaction temperature of 95 °C in an aqueous solution using Au NRs as sacrificial templates.

Acknowledgments

We thank Dai Nippon Toryo Co., Ltd. for

supplying Au NRs used in this study. This work was supported by JSPS KAKENHI Grant Numbers JP25286003, JP25550056.

References

1) J. Gong, *Chem. Rev.,* 112, 2987 (2012).
2) S. Leenders,. Leenders, R. Gramage-Doria, B. Bruin, and J. Reek, *Chem. Soc. Rev.*, 44, 433 (2015).
3) M. N. Liz-Marzán, C. J. Murphy, and J. Wang, *Chem. Soc. Rev.*, 43, 3820 (2014).
4) L. K. Bogart, G. Pourroy, C. J. Murphy, V. Puntes, T. Pellegrino, D. Rosenblum, D. Peer, and R. Lévy, *ACS Nano*, 8, 3107 (2014).
5) P. K. Jain, X. Huang, I. H. El-Sayed, and E. A. El-Sayed, *Acc. Chem. Res.*, 41, 1578 (2008).
6) Y. Xia, W. Li, C. M. Cobley, J. Chen, X. Xia, Q. Zhang, M. Yang, E. C. Cho, and P. K. Brown, *Acc. Chem. Res.*, 44, 914 (2011).
7) M. C. Daniel and D. Astruc, *Chem. Rev.*, 104, 293 (2004).
8) D. Kim, Y. W. Lee, S. B. Lee, and S. W. Han, *Angew. Chem. Int. Ed.*, 51, 159 (2012).
9) K. D. Gilroy, A. Ruditskiy, H.-C. Peng, D. Qin, and Y. Xia, *Chem. Rev.*, 116, 10414 (2016).
10) S. W. Kim, M. Kim, W. Y. Lee, and T. Hyeon, *J. Am. Chem. Soc.*, 124, 7642 (2002).
11) Y. G. Sun, B. Mayers, and Y. Xia, *Adv. Mater.*, 15, 641 (2003).
12) S. E. Skrabalak, J. Chen, Y. Sun, X. Lu, L. Au, C. M. Cobley, and Y. Xia, *Acc. Chem. Res.*, 41, 1587 (2008).
13) C. M. Cobley and Y. Xia, *Mater. Sci. Eng., R*, 70, 44 (2010).
14) X. Xia, Y. Wang, A. Ruditskiy and Y. Xia, *Adv. Mater.*, 2013, 25, 6313 (2013).
15) R. Long, S. Zhou, B. J. Wiley, and Y. Xiong, *Chem. Soc. Rev.,* 43, 6288 (2014).
16) G. Mettela and G. U. Kulkarni, *Nano Res.*, 8, 2925 (2015).
17) F. Merkoçi, J. Patarroyo, L. Russo, J. Piella, A. Genç, J. Arbiol, N. G. Bastús, and V. Puntes, *Mater. Today Adv.*, 5, 100037 (2020).
18) M. Tsuji, T. Kidera, A. Yajima, M. Hamasaki, M. Hattori, T. Tsuji, and H. Kawazumi, *CrystEngComm*, 16, 2684 (2014).
19) M. Tsuji, M. Hamasaki, A. Yajima, M. Hattori, T. Tsuji, and H. Kawazumi, *Mater. Lett.*, 121, 113 (2014).
20) Y. G. Sun and Y. Xia, *J. Am. Chem. Soc.*, 126, 3892 (2004).
21) Y. G. Sun and Y. Xia, *Adv. Mater.*, 16, 264 (2004).
22) Y. G. Sun, B. Wiley, Z.-Y. Li, and Y. Xia, *J. Am. Chem. Soc.*, 126, 9399 (2004).
23) M. Tsuji, Y. Nakashima, A. Yajima, and M. Hattori, *CrystEngComm*, 17, 6955 (2015).
24) Y. Niidome, K. Nishioka, H. Kawasaki, and S. Yamada, *Chem. Commun.*, 2376 (2003).
25) D. Seo, C. I. Yoo, I. S. Chung, S. M. Park, S. Ryu, and H. Song, *J. Phys. Chem. C*, 112, 2469 (2008).
26) M. Tsuji, N. Nakamura, M. Ogino, K. Ikedo, and M. Matsunaga, *CrystEngComm*, 14, 7639 (2012).
27) M. B. Cortie and A. M. McDonagh, *Chem. Rev.*, 111, 3713 (2011).
28) M. Tsuji, K. Ikedo, K. Uto, M. Matsunaga, Y. Yoshida, K. Takemura, and Y. Niidome, *CrystEngComm*, 15, 6553 (2013).
29) A. R. Denton and N. W. Ashcro, *Phys. Rev. A*, 43, 3161 (1991).
30) E. Carbó-Argibay, B. Rodríguez-González, S. Gómez-Graña, A. Guerrero-Martínez, I. Pastoriza-Santos, J. Pérez-Juste and L. M. Liz-Marzán, *Angew. Chem., Int. Ed.,* 49, 9397 (2010).
31) B. Goris, S. Bals, W. Van den Broek, E. Carbó-Argibay, S. Gómez-Graña, L. M. Liz-Marzán, and G. Van Tendeloo, *Nat. Mater.*, 11, 930 (2012).
32) M. Tsuji, K. Takemura, C. Shiraishi, K. Ikedo, K. Uto, A. Yajima, M. Hattori, Y. Nakashima, K. Fukutomi, K. Tsuruda, T. Daio, T. Tsuji, and S. Hata, *J. Phys. Chem. C*, 119, 10811 (2015).
33) Y. Yoshida, K. Uto, M. Hattori, and M. Tsuji, *CrystEngComm*, 16, 5672 (2014).